

Highlights

Low-cost optical multi-wavelength sensor for accurate real-time state-of-charge monitoring in vanadium flow batteries

Ange A. Maurice, Pablo A. Prieto-Díaz, Marcos Vera

- Low-cost mini optical sensor for real-time State of Charge (SoC) and vanadium concentration monitoring
- System assembly cost under € 150
- Optimized sensor design by tuning channel number and wavelength position
- 6 channels in the range 445–630 nm
- Overall calibration accuracy of 70 mM for vanadium concentration and 2.4% for the SoC

Low-cost optical multi-wavelength sensor for accurate real-time state-of-charge monitoring in vanadium flow batteries

Ange A. Maurice^{a,*}, Pablo A. Prieto-Díaz^a, Marcos Vera^{a,*}

^a*Departamento de Ingeniería Térmica y de Fluidos, Universidad Carlos III de Madrid, Avd. de la Universidad 30, Leganés, 28911, Madrid, Spain*

Abstract

We presents a novel, low-cost optical sensor for accurate real-time monitoring of state of charge (SoC) and total vanadium concentration in vanadium flow batteries. Using only six discrete wavelengths, the sensor achieves precision comparable to full-spectrum methods while significantly reducing equipment costs and complexity. A general deconvolution method is used to measure both the SoC and the total vanadium concentration in both the posolyte and negolyte, with calibration covering concentrations from 1.2 to 1.8 M. We achieve an overall accuracy of 2.4% for the SoC and 70 mM for the total vanadium concentration. Additionally, an optimization study is proposed to determine the optimal number and placement of spectral channels, providing a basis for designing tailored optical sensors for vanadium electrolytes.

Keywords: UV-Vis spectroscopy, Vanadium Redox Flow Battery, Low-Cost Optical Sensor, State of Charge, Electrolyte Concentration

1. Introduction

Energy storage systems play a key role in the transition toward renewable energy, addressing the intermittency of solar and wind power and enabling more reliable and sustainable electricity grids [1]. Among the various energy storage technologies, electrochemical energy storage stands out for its versatility, scalability, and wide range of applications, from portable electronics to grid-scale systems [2]. In this context, redox flow batteries (RFBs) offer a promising alternative to conventional batteries for grid-scale energy storage due to their unique ability to decouple power and energy capacities [3]. Unlike solid-state batteries, RFBs store energy in liquid electrolytes, making them inherently scalable and well-suited for large-scale, stationary applications [4, 5].

Among RFB technologies, vanadium redox flow batteries (VRFBs) stand out due to their good performance and strong near-term commercialization potential [6]. They offer several advantages that make them a promising large-scale stationary energy storage solution: high round-trip energy efficiency, excellent scalability, long cycle life, deep discharge capability, and high safety compared to other types of batteries. However, a significant drawback of VRFBs is their capacity decay during cycling, mainly caused by ion crossover [7], hydrogen evolution [8], or imperfect electrolyte

*Corresponding authors

Email addresses: amaurice@pa.uc3m.es (Ange A. Maurice), pabloangel.prieto@uc3m.es (Pablo A. Prieto-Díaz), marcos.vera@uc3m.es (Marcos Vera)

mixing in the tanks [9]. This makes the total vanadium concentration and the State of Charge (SoC) to drift away from the ideal symmetric state between the negative and positive electrolytes, creating an undesired charge imbalance [10].

One of the biggest challenges related to the vanadium flow battery is to diagnose such an imbalance by accurately and independently measuring the State of Charge (SoC) of the negative and positive half-cells, that is, the relative concentration of charged species on the negative side (anolyte, V^{II}/V^{III}) and the positive side (catholyte, V^{IV}/V^V) [11]. Following standard practice, the four oxidation states of vanadium V^{2+} , V^{3+} , VO^{2+} , and VO_2^+ are denoted here as V^{II} , V^{III} , V^{IV} , and V^V , or with subscripts $i = \{2, 3, 4, 5\}$. As shown in Table 1, the concentrations C_i of these species determine both the SoC of each half-cell and the total concentration C of vanadium ions.

A direct, non-invasive method for measuring the SoC in VRFBs is through Ultraviolet-Visible (UV-Vis) absorbance spectroscopy. UV-Vis spectroscopy has been widely explored in the literature for studying the chemistry of vanadium electrolytes as well as for measuring the SoC. Early investigations, such as those by Blanc et al. [12], laid the groundwork for understanding the complex chemistry of the posolyte, along with subsequent contributions by other groups [13, 14]. The method has been applied both offline and online to determine the state of charge (SOC) of vanadium electrolytes [15, 16, 17, 18]. Most of these works employ calibration procedures based on empirical models, which makes them prone to measurement drifts. More recently, Loktionov et al. [19] proposed a disruptive approach based on the spectral deconvolution method, searching for the individual absorbance contribution of each vanadium compound. Building on their method, we further refined, simplified and extended the deconvolution method to a wider range of concentrations, confirming its strength and robustness in measuring the total vanadium concentration and SoC independently [20].

Nonetheless, UV-visible spectroscopy techniques rely on expensive optical systems, including light sources, spectrometers, optical cuvettes/cells, optical fibers, etc. Typically, the absorbance spectra obtained with these systems are “continuous”, containing at least 3000 data points and spanning a broad wavelength range (300 to 1000 nm). In this study, we propose to drastically lower the number of channels, effectively using a discrete spectrum of only 6 channels. This spectrum can be acquired using a low-cost spectrometer typically sold for less than € 30 (e.g., the

Electrolyte mixture		
Variable	Negolyte V^{II}/V^{III}	Posolyte V^{IV}/V^V
C	$C_2 + C_3$	$C_4 + C_5 + 2C_{45}$
SoC	$\frac{C_2}{C_2 + C_3}$	$\frac{C_5 + C_{45}}{C_4 + C_5 + 2C_{45}}$

Table 1: Definition of the total vanadium concentration C , mole fractions X_i , and SOC for the posolyte and the negolyte under study as a function of the molar concentration of the four vanadium ions C_i , $i = \{2, 3, 4, 5\}$. In the V^{IV}/V^V mixture C_{45} denotes the concentration of the 1:1 stoichiometric mixed-valence complex $V_2O_3^{3+}$ at equilibrium with V^{IV} and V^V as described in [12]

AS7341 multi-spectral digital sensor from ams-OSRAM). The existence of such devices presents an opportunity to develop an affordable sensor for vanadium redox flow batteries, enhancing online diagnostic capabilities and improving the cost-benefit ratio, an essential factor for the widespread adoption of this technology.

It is worth mentioning that several optical sensors have already been developed for vanadium flow batteries, predominantly single-channel designs [21, 22, 23, 17, 24]. These sensors typically detect colour changes using a photodiode and are valued for their low cost and high simplicity. However, their limited spectral information poses significant challenges. Specifically, they are unable to address calibration drifts due to variations of the total concentration C that are critical for maintaining long-term measurement robustness. These limitations are particularly pronounced in the posolyte due to its non-linear spectral response.

In this work, we maintain the cost-effectiveness of these systems while achieving robustness comparable to that of continuous UV-Vis spectrometers. In particular, we present a low-cost discrete absorbance measurement system, designed using a multi-channel optical sensor, a LED light source, a polymer microfluidics chip and a Raspberry Pi [25]. The rest of the components are 3D printed, amounting to an approximate total cost of € 150. To verify the system's ability to measure both the SoC and the concentration, we measured a total of 66 samples with known SoC and concentrations (ranging from 1.21 to 1.82 M). We then applied the same calibration procedure outlined in our previous study [20] based on a deconvolution method. For details on the calibration algorithm, the reader is referred to our prior work for further clarification.

The proposed system, based on a commercial off-the-shelf optical sensor, demonstrates reliable performance but is limited by the fixed positions of its spectral channels, which are not optimized for the particular optical properties of vanadium electrolytes. To address this limitation, we explore the challenge of optimizing both the number and placement of spectral channels to minimize measurement error. The objective is to propose a new optical sensor with strategically selected channels, enabling precise measurement of total vanadium concentration and SoC in VRFBs. By identifying the most effective wavelengths and minimizing the required number of channels, we aim to achieve the optimal balance between accuracy and affordability, paving the way for a disruptive customized optical sensor for VRFBs.

The paper is organized as follows. In Section 2 we describe the sensor design, the measurement protocol and the procedures employed to prepare the calibration samples. Section 3 presents the acquired data, a summary of the deconvolution method and the result of the calibration. Section 4 discusses the optimization study, detailing the methodology used to identify the optimal number and placement of spectral channels and the resulting performance improvements. Finally, in Section 5, we summarize the key findings and draw the conclusions.

2. Experimental

2.1. Sample preparation

The sample preparation protocol employed in this study follows the methodology outlined in our previous work [20], with a brief summary provided below for completeness. Calibrating UV-Vis spectroscopic methods requires the precise preparation of single-species reference electrolytes and their mixtures. This was achieved by carefully pipetting, mixing, and diluting reference solutions of V^{II} , V^{III} , V^{IV} , and V^{V} , while adjusting the vanadium concentration and the state of charge (SOC)

as needed. Using deionized water and a high-precision scale, we ensured a pipetting accuracy of 0.4%. For calibration, we prepared 66 samples across three vanadium concentrations (1.82 M, 1.52 M, and 1.21 M), with SOC's ranging from 0% to 100%. Concentrations below 1.21 M were excluded due to their limited industrial relevance.

The reference solutions of the four vanadium electrolytes were prepared by electrochemical charging of an equimolar V^{III}/V^{IV} commercial solution (Oxkem Limited, UK) with a vanadium concentration of 1.82 M and an acid concentration of 4.6 M. A key advantage of this preparation method, as detailed in our previous work, lies in the use of spectrophotometric titration with real-time spectral monitoring. This approach enables the precise identification of inflection points in the absorbance data, thus facilitating the accurate detection of pure electrolyte solutions [20]. Additionally, we also employed this titration approach to verify the total vanadium concentration (1.82 M) of the commercial electrolyte using Potassium Permanganate as titrant [26].

2.2. Sensor design

The absorbance of the samples is measured via a multi-wavelength optical sensor (415-910 nm) (AS7341 ams-OSRAM, Austria) mounted on a breakout board (Pimoroni, UK). Further details of the optical sensor, including an optical channel summary with channel numbers, center wavelengths, and full width at half maximum, can be found in the product datasheet [27]. The light source is a white LED Backlight module (12 mm \times 40 mm, Adafruit, USA) with a diffuser. A microfluidic chip is used as the flow cuvette (Fluidic 620, Microfluidic Chipshop, Germany). The chip has 16 separate channels of varying depth (length/width/depth, 18/2/0.8–0.1 mm). For absorbance measurements, the depth of the chosen microfluidic channel is the path length of the flow cuvette. In this work, we only used the 0.15 mm deep channel to account for the high absorbance of the polysolite in the 40–50% SoC range. The microfluidic chip is connected via Mini Luer rubber fittings with standard PTFE microfluidic tubes (OD/ID, 1.6/0.8 mm).

Figure 1(a,b) presents a 3D view and a cross-sectional view of the assembled system while (c) and (d) show a close-up view of the measuring system, both in photo and in 3D. The black inner support part serves three main functions: i) to secure the AS7341 board in place, ii) to block external light from reaching the sensor, and iii) to align the sensor with the microfluidic chip. The support features a square aperture (1.8 mm wide) that allows the light from the source to reach the optical sensor after crossing the microfluidic chip. Although placing the sensor closer to the light source would increase the amount of light it receives, the design includes a 10.7 mm clearance to accommodate the tube fittings. This reduction in light is compensated by increasing the measurement integration time. The system is held in place for measurements by a white frame with a mounting bolt. For data acquisition, the sensor is connected to a Raspberry Pi Zero, paired with a 320 \times 280 pixel screen (Display HAT Mini, Pimoroni, UK). The sensor is designed to function as a standalone unit, capable of plotting absorbance and measuring the electrolyte's SoC using a pre-loaded calibration without the need of an external computer.

2.3. Measurements

The absorbance A is calculated via

$$A = -\frac{1}{l} \log \left(\frac{I}{I_{\text{ref}}} \right) \quad (1)$$

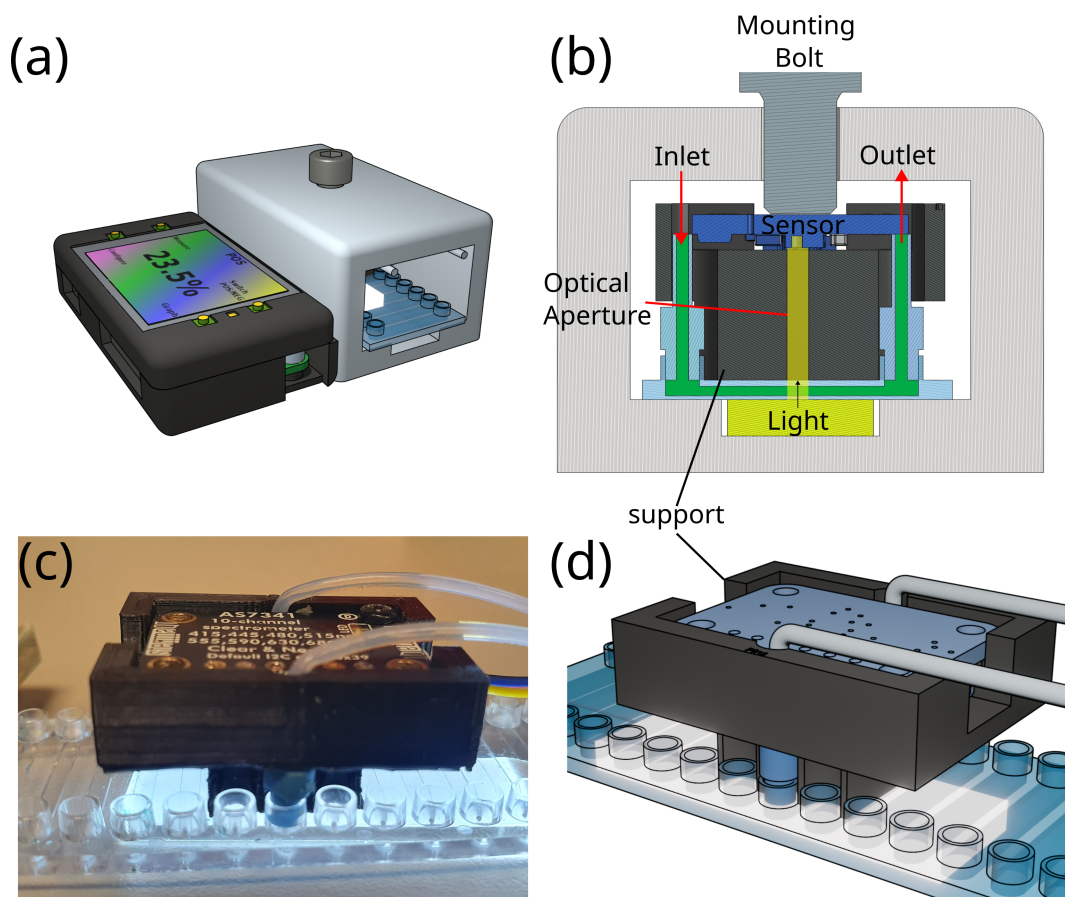


Figure 1: (a) 3D view of the final vanadium sensor design: The measurement is performed via a Raspberry Pi Zero connected to a screen (Black box). The white frame is a support holding the measuring system in place. (b) Cross sectional view of the measuring area, the green area represents the vanadium electrolyte flowing in and out of the chip (c) Photograph of the measuring system without the support with its corresponding 3D view in (d).

where I is the light intensity (raw data units) measured with the electrolyte, I_{ref} is the light intensity measured with pure water, used as reference, and l is the path length, chosen as 0.15 mm in this work. As an illustrative example, Table 2.3 shows the light intensity (in raw data units) obtained by measuring a 1.82 M solution of pure V^{IV} ; the reference intensity was acquired with pure water and the dark signal was measured with no light exposure. The zero values observed in the dark signal confirm that neither external light nor internal noise was detected. For this reason D is not included in equation 1. The total measurement time is ≈ 10 s, including 5 s of integration time.

Figure 2(a) shows the raw spectrum of the LED source obtained with a laboratory grade UV-Visible spectrometer (Goyalab Indigo, France). The emission spectrum of the LED ranges approximately from 420 to 700 nm. Consequently, the counts detected by channels F1 - 415 nm and F9 - 910 nm (Table 2.3) are likely to arise from measurement noise, as mentioned below. Figure 2(b) shows an example of the absorbance spectrum of a pure V^{IV} electrolyte acquired using the multichannel sensor (blue curve) and a commercial spectrometer (red curve, Flame T-VIS-NIR-ES, Ocean Insight, USA). Although the spectra are similar in shape, significant distortions

Channel - Center wavelength	Counts		
	Measurement I	Reference I_{ref}	Dark I_{D}
Visible (VIS)			
F1 - 415 nm	848.0	888.0	0
F2 - 445 nm	4774.0	4813.0	0
F3 - 480 nm	1485.0	1565.0	0
F4 - 515 nm	3391.0	3659.0	0
F5 - 555 nm	3476.0	4337.0	0
F6 - 590 nm	2214.0	3409.0	0
F7 - 630 nm	1249.0	2265.0	0
F8 - 680 nm	478.0	890.0	0
Near Infrared (NIR)			
F9 - 910 nm	232	340	0

Table 2: Raw data counts measured using a solution of pure V^{IV} at 1.82 M, I , reference data measured with pure water, I_{ref} , and dark data measured without light, D . The channel number and center wavelength are obtained from the product datasheet [27].

are observed between the “ideal” spectrum and the one measured with the multichannel sensor. These distortions are inherent to such devices and arise from factors such as optical interferences, imperfect filters, and internal reflections. These issues result in spectral responsivity overlapping not only with adjacent channels but also with others further along the spectrum. Whereas the reference division in (1) helps mitigate some of these effects, they remain significant—particularly for the F8 - 680 nm channel, which exhibits significantly lower absorbance values. Therefore, as shown by the green area in Figure 2(b), channels F1 - 415 nm, F8 - 680 nm, and F9 - 910 nm are excluded from further analysis for the remainder of this study, reducing the effective channel count to six, spanning the range from 445 to 630 nm.

3. Results and calibration

3.1. Multichannel spectra

Figure 3 shows the acquired anolyte and catholyte spectra between 0% and 100% SoC. The changes observed as the state of charge increases are consistent with both the literature [12] and our previous data [20]. The absorbance function of the spectra can be modelled as

$$A_{\text{neg}} = [\epsilon_2 \text{SoC} + \epsilon_3 (\text{SoC} - 1)] C \quad (2)$$

$$A_{\text{pos}} = \epsilon_4 [(\text{SoC} - 1)C - C_{45}] + \epsilon_5 [(C\text{SoC} - C_{45})]^k + \epsilon_{45} C_{45} \quad (3)$$

where A_{neg} and A_{pos} are the absorbances of the negolyte and the posolyte per unit of path length (in this work, cm^{-1}), and ϵ_i represents the molar absorptivity of each pure vanadium compound i . Whereas the negolyte exhibits a linear behavior consistent with a binary mixture absorption model, the posolyte is known to contain a third component: a highly absorbing mixed-valence compound,

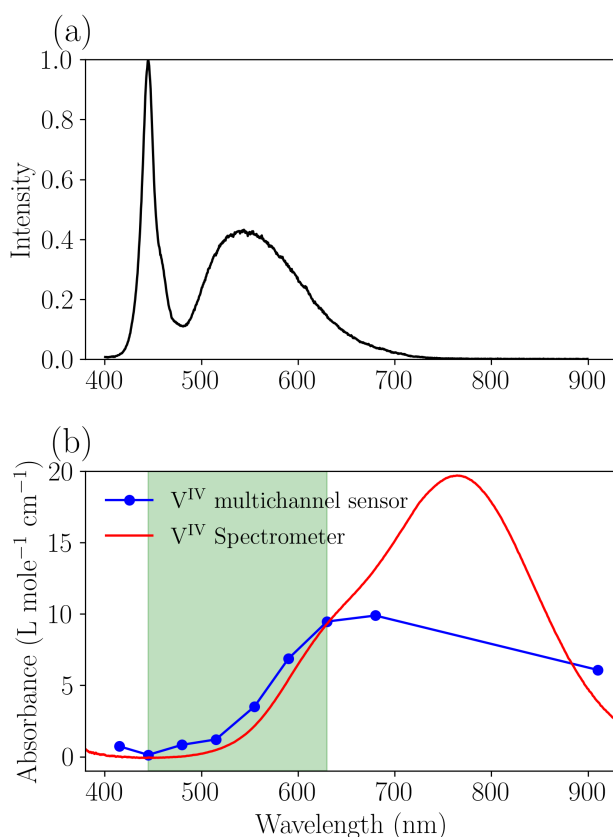


Figure 2: (a) Absorbance spectrum of the LED light acquired with a UV-Visible Spectrometer (b) Absorbance spectra of a pure 1.82 M V^{IV} electrolyte acquired with the multichannel sensor (blue) and a UV-Visible spectrometer. The green area represents the chosen range of wavelength retained for this study.

$V_2O_3^{3+}$, formed between V^{IV} and V^V , denoted here by subscript $i = 45$ [12]. In Eq. 3, $k = 2.09$ and (C_{45}, ϵ_{45}) represent the concentration and molar absorptivity of this complex, respectively. C_{45} depends on C and SoC according to

$$C_{45} = \frac{1 - \sqrt{1 - 4\chi^2 \text{SoC}(1 - \text{SoC})C^2}}{2\chi} \quad (4)$$

where $\chi = K_c/(K_c C + 1)$ with $K_c = 0.89$. The given values of k and K_c are extracted from our previous work [20].

3.2. State of Charge Calibration

To interpret the spectra and relate them to SoC values, we perform spectral deconvolution. Although this method is thoroughly described in [20], a concise summary is provided here for completeness. The process involves mathematically extracting the individual contributions of each component from the observed composite spectrum, thereby enabling the quantification of their respective concentrations and absorbances. The deconvolution proceeds by fitting the best pair

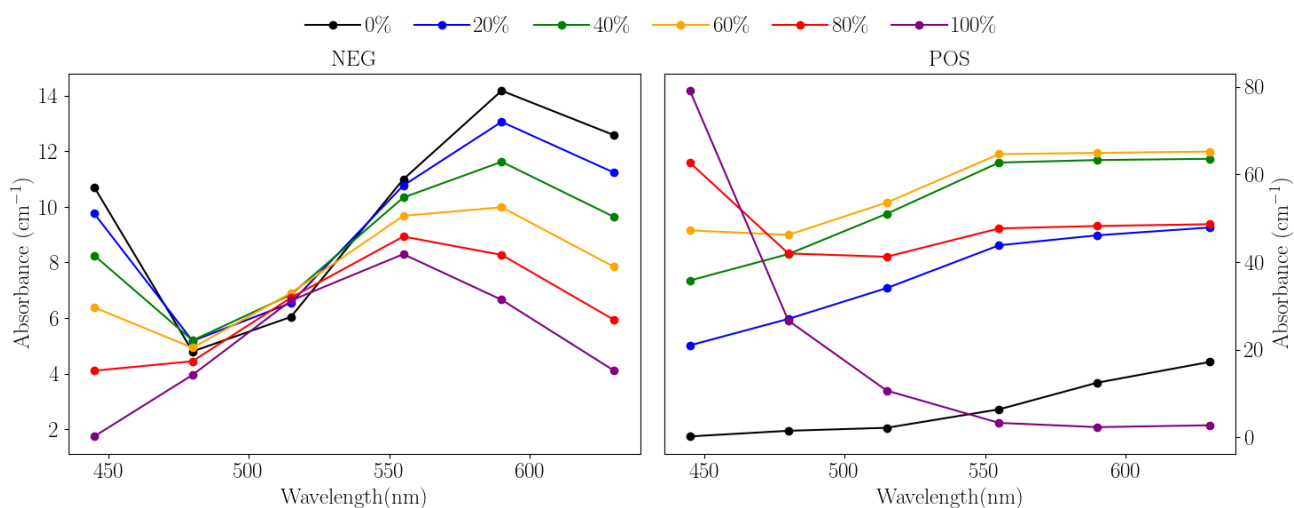


Figure 3: Absorbance spectra acquired for the negolyte and the posolyte varying the SoC for a total vanadium concentration of 1.82 M and an optical path of 0.15 mm.

(SoC, C) that minimizes the sum of squared errors

$$\sum_{\lambda} \{A_{\text{exp}} - A_{\text{pos/neg}}\}^2 \quad (5)$$

between the experimentally measured absorbance A_{exp} and the modelled absorbances, either A_{neg} or A_{pos} , given by Eqs. (2) and (3). We performed this regression using a minimization function, e.g., the `scipy.optimize.minimize` function in Python or the `fmincon` function in MATLAB, both of which converge to an optimal solution.

Figure 4 shows the results of the deconvolution process for the negolyte (a, c, d) and the posolyte (b, e, f). Some illustrative spectral fit examples are shown in (a, b) for SoC = 50% and $C = 1.82$ M. The dashed line represent the individual absorbance contribution of the pure compounds. The sum of these contributions yields the fitted curve (red) that is in good agreement with the experimental curve (black). For each spectrum, the minimization yields a set of predicted values (C_{P} , SoC_P) that we compare to the true values (C_{T} , SoC_T) that we know from our sample preparation (Section 2.1). Figure 4 (c, d, e, f) show the calibration curves of the negolyte (c, d) and the posolyte (e, f). These scatter plots compare the predicted values to the true values, with black dots representing results across all concentrations. Ideally, with 100% calibration accuracy, the predicted values would lie along the $y = x$ blue line. Deviations from this line reflect calibration inaccuracies and measurement errors. To assess accuracy, the Root Mean Square Error (RMSE) was calculated for all concentrations, as detailed in Table 3. For the negolyte and the posolyte, the RMSE were respectively 1.54% and 3.25% for the SoC and 41 mM and 99 mM for the concentration. As should be expected, the positive calibration exhibits a higher error due to its non-linear spectral response and the presence of the complex. We also compared the errors obtained in this study with those from our previous work, where calibration was performed using continuous spectra collected with a commercial UV-Visible spectrometer. Although the errors from the continuous calibration were approximately half as large, this difference is relatively small, especially considering the leap

from 6 to 3600 channels. This highlights the complexity of the relationship between calibration error, channel position, and number of channels. In other words, a discrete spectrum can hold substantial analytical information even with a limited number of channels. Nonetheless, considering the technological simplicity and cost-effectiveness of this system, these results are impressive and provide a strong proof of concept for developing multi-wavelength optical sensors for VRFBs.

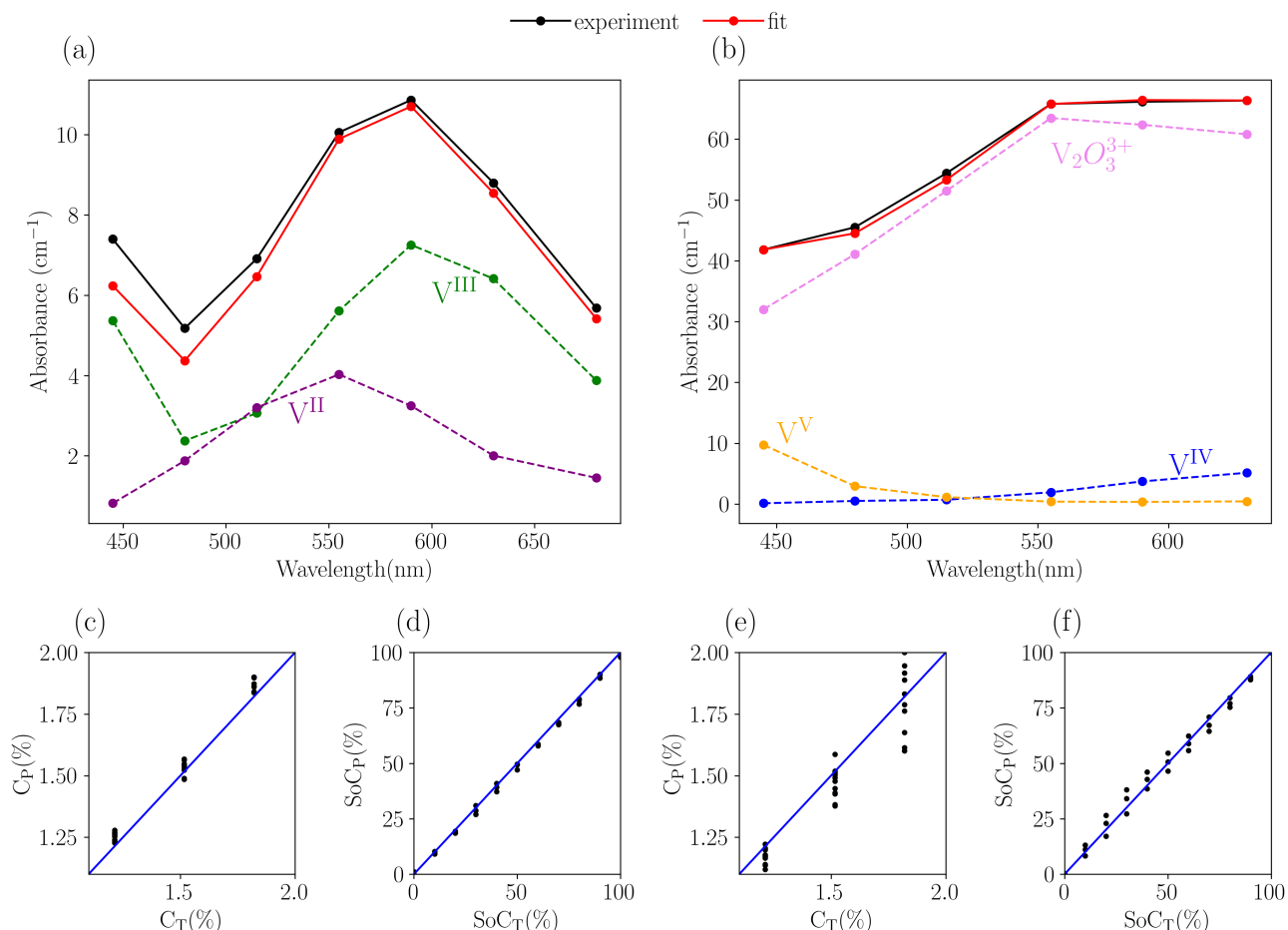


Figure 4: Examples of the deconvolution process performed for the negolyte (a) and the posolyte (b) at SoC = 50% and $C = 1.82$ M. The dashed lines represent the spectral contributions of the pure compounds. (c, d, e, f) Calibration curves representing the predicted values versus the true values for the SoC and the total concentration. (c, d) show the results obtained for the negolyte while (e, f) represent the posolyte. The 100% accuracy line ($y = x$) is plotted in blue.

4. The optimal channel configuration

The previous results were obtained using a commercial off-the-shelf optical sensor using six fixed wavelength channels, compatible with the chosen light source. However, these wavelengths were not specifically tailored for the optical diagnosis of vanadium electrolytes, which highlights the potential for design optimization. This section explores how to achieve the optimal sensor

design by selecting the minimum number of channels and positioning them at optimal wavelengths to minimize calibration error while maintaining high accuracy.

4.1. Genetic algorithm

We used a genetic algorithm to optimize the location of a specified number of channels. This method also allows us to identify the global minimum, avoiding local minima. The genetic algorithm uses a population size of 100 candidate solutions, each candidate being a group with a specified number of wavelengths. At each step, the best (that is, those who produce the lowest mean square error) 5 children pass to the next generation, the next 72 children cross their data to vary the genes (weighted by a random number from a Laplace distribution, see [28]) and the other 23 are again randomly generated. All candidate solutions comply with two rules: adjacent wavelengths are distanced by more than 5 nm, and they must remain within 440-900 nm. The minimum number of wavelengths is set to two, as determining both Soc and C is impossible with one value. For each candidate solution, we gauge its performance by applying the spectral deconvolution method discussed above. To do so, we simulate an ideal multi-wavelength sensor by using the "continuous" spectral database reported in [20], discretized according to the corresponding wavelength. Note that this approach omits optical interferences or other distortions that occur in a real sensor. The procedure is computed using the MATLAB optimization toolbox.

4.2. Results

Figure 5 shows the optimization results for the negolyte (left) and the posolyte (right). To better highlight the strength of wavelength customization, we compare our genetically optimized results (black curve) with a straightforward approach consisting in varying the channel number using channels equidistantly spaced without placement optimization (blue curve). Additionally, the red marker represents the RMSE obtained when using the low-cost optical sensor described in the previous section.

For the negolyte, both the RMSE of concentration (Fig. 5a) and SoC (Fig. 5b) remain low when using the genetically optimized wavelength positions (black lines), regardless of the number of wavelengths selected. This is expected since the negolyte exhibits a linear spectral response, allowing low RMSE values to be achieved with just two strategically chosen wavelengths—specifically those with high absorbance variation (see Fig. 5c)—as when using the full spectrum [20]. The algorithm finds two optimal regions for wavelength placement: at high wavelengths (>850 nm), where V^{III} does not absorb and the absorbance is dominated by V^{II} ; and around 600 nm, near the global

Spectrum type	Mixture	RMSE C	RMSE SoC
6 channels (this work)	Negolyte	41 mM	1.54%
	Posolyte	99mM	3.25%
Continuous (Maurice et al. [20])	Negolyte	22mM	0.74%
	Posolyte	37mM	1.57%

Table 3: Root Mean square errors calculated for the posolyte, the negolyte, the total concentration C and the SoC. Results from our previous work carried out with continuous spectra are added for comparison.

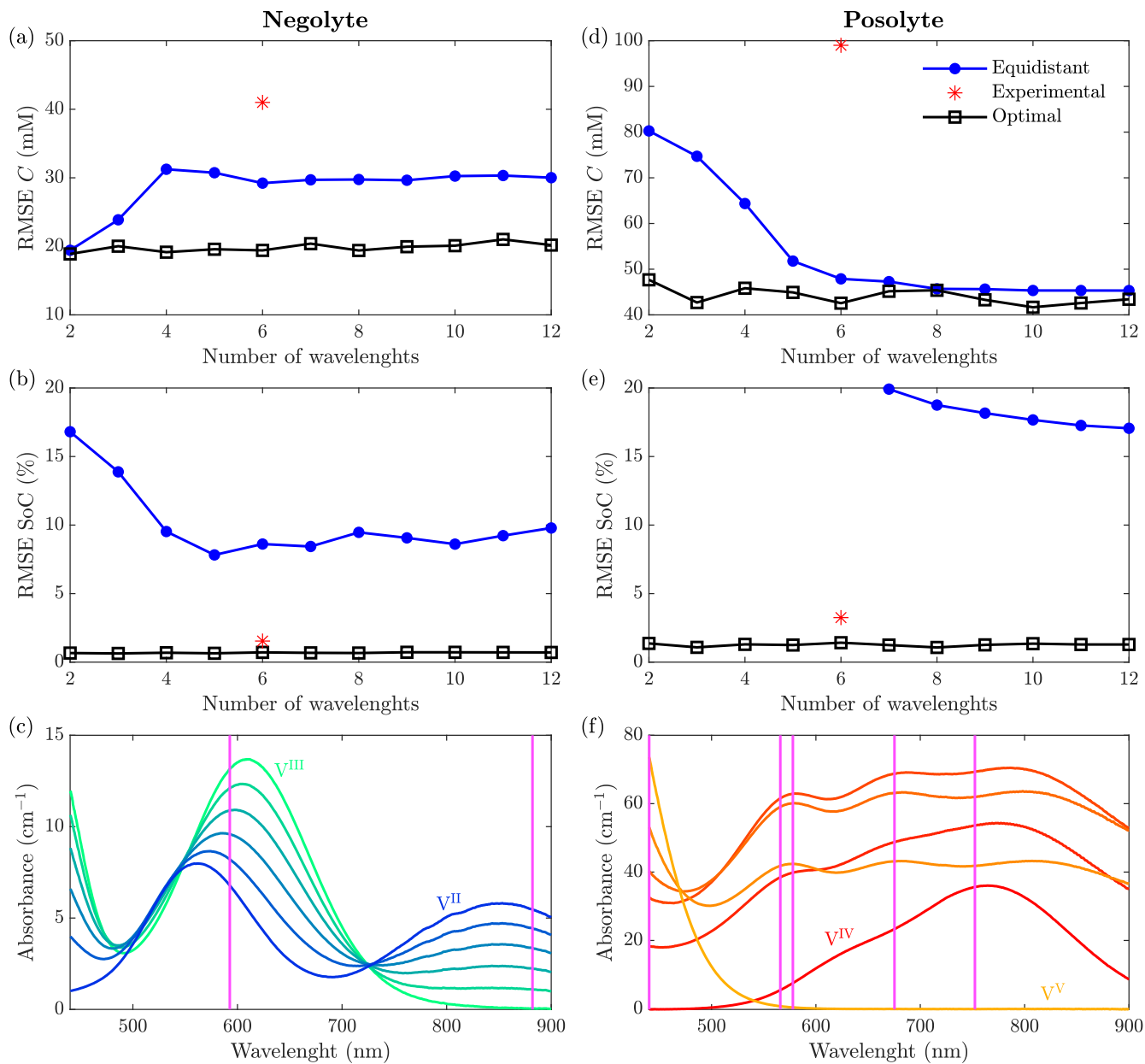


Figure 5: RMSE of the total vanadium concentration (a, d) and SoC (b, e) computed using different numbers of channels in the optimal wavelengths (blue lines) and at equidistant lengths (black lines), in addition to the experimental results (red asterisk); reference spectra for different SoCs obtained from [20] (c, f) with the chosen number of wavelengths and their positions as vertical lines. Plots on the left (a, b, c) correspond to the negolyte and the ones on the right (d, e, f) to the posolyte.

maximum of the spectrum, with its exact position varying based on the SoC. As the number of wavelengths increases, they concentrate within these two regions, where the spectral variation is more pronounced, and to a lesser extent around 690 nm, where V^{II} shows a local minimum. In contrast, channels placed at equidistant positions (blue lines) result in higher RMSE values as some of them may fall in regions of minimal spectral change.

For the posolyte (right), the RMSE values remain close to those obtained with the entire spectrum, although they are slightly higher when using only two channels (Fig. 5d and 5e). The algorithm identifies optimal placements up to 800 nm, as the spectra signal of each specie vary. Notably, 440 nm appears as an optimal placement for identifying the absorbance of V^V , which reaches its maximum at this lower wavelength (Fig. 5f). Moreover, this is the only region of the spectrum directly proportional to both the total vanadium concentration and the SoC, enabling a low RMSE with the addition of just one additional channel. This additional wavelength is placed around 760 nm, corresponding to the global maximum of the V^{IV} spectrum. Subsequent optimal wavelengths are placed near local minima and maxima of $V_2O_3^{3+}$, resulting in slightly lower RMSE values for SoC (Fig. 5e). For concentration (Fig. 5d), adding more wavelengths reduces the RMSE to values comparable to those obtained using the full spectrum, showing a more significant improvement than for the other RMSE metrics. As observed with the negolyte, equidistantly placed channels result again in higher RMSE values, particularly for the SoC, as the information about V^V is concentrated at lower wavelengths.

In both electrolytes, the experimental RMSE values are expectedly higher than those obtained numerically for the total vanadium concentration and slightly higher for the SoC. These results highlight the strength of configuring the wavelengths of an optical absorbance sensor for RFBs, showcasing the potential design improvements that could be made. We demonstrate that calibration errors close to the full spectrum can be achieved using fewer than 6 channels. Nonetheless, we acknowledge that part of the difference between optimal and experimental RMSE could be partially due to experimental errors (sample preparation, spectral distortions). In addition, our experimental sensor only detects wavelength up to 680 nm compared to the 900 nm limit provided in the optimization. With a limited number of channels, these spectral distortions might be difficult to detect, which could pose challenges for recalibrating the sensor. Despite these limitations, these results provide a guide for future sensor designs.

5. Conclusions

This work presents the development and evaluation of a low-cost, multi-wavelength optical sensor for real-time monitoring of the SoC and total vanadium concentration in VRFBs. Using a led light source and a commercial off-the-shelf (COTS) multi-wavelength sensor with six compatible spectral channels ranging from 445 to 630 nm, we demonstrate that accurate measurements can be achieved without relying on expensive full-spectrum UV-Vis spectroscopy systems. Using spectral deconvolution and a calibration based on 66 carefully prepared samples, the sensor demonstrated its ability to quantify the SoC and the total vanadium concentration with root mean square errors of 2.4% and 70 mM, respectively. These results confirm that discrete spectral sensors can effectively capture the essential optical features of vanadium electrolytes absorbance spectra, offering a reliable alternative to traditional full-spectral methods. The proposed system is characterized by its cost-effectiveness and practical design. With a total assembly cost of less than € 150, it provides a significant reduction in the financial and technical barriers typically associated with SoC monitoring in VRFBs. This makes the technology more accessible and scalable, offering a promising solution for energy storage systems where cost-effectiveness is critical.

In addition to the system design, based on a COTS optical sensor, an optimization study has been performed to determine the optimal location and number of spectral channels. The results

demonstrate that, using less than 12 channels, measurement errors could potentially be reduced to levels comparable to those achieved with continuous spectra. This study provides a framework for tailoring sensor designs to the specific optical properties of vanadium electrolytes, allowing for increased accuracy while maintaining system simplicity. A key limitation of the optimization study is that it yields different optimum designs for the negolyte and posolyte. Although this provides valuable insight it also highlights a key limitation: the current approach requires *a priori* knowledge of the specific electrolyte type. Future research should aim to develop a general-purpose sensor capable of analyzing any electrolyte composition without prior distinction between negolyte and posolyte. Such a sensor would be especially useful for electrolyte rebalancing operations, as it would allow equimolar mixtures V^{III}/V^{IV} to be obtained with greater precision and consolidate the system into a single versatile device.

In conclusion, this study provides a strong proof of concept for the use of low-cost optical multi-wavelength sensors in VRFB diagnostics, paving the way for more accessible and scalable solutions in energy storage applications. The experimental results offer valuable insights into the system's limitations, identifying challenges such as spectral distortions and channel overlaps, which are inherent to low-cost sensors. These findings underscore the need for further advancements in sensor design, aiming in particular to mitigate such distortions and incorporate self-calibration strategies. Furthermore, the channel optimization study provides an effective framework that can guide the design and development of next-generation, low-cost optical sensors tailored to VRFBs and other energy storage applications.

Data availability

The calibration data and software tools developed in this work are publicly shared in an online repository (Github), ensuring transparency and enabling reproducibility of the results.

Declaration on the use of generative AI

During the preparation of this work, we used ChatGPT in order to enhance and improve text flow. After using this tool/service, we reviewed and edited the content as needed and assume full responsibility for the content of the publication.

Acknowledgments

We would like to thank Ángel González Ahijado, patent technician at the Entrepreneurship and Innovation Support Service of Universidad Carlos III de Madrid, for useful discussions regarding the optimization of the channel configuration.

Author contributions

Ange A. Maurice: Conceptualization, Methodology, Software, Validation, Formal analysis, Investigation, Resources, Data Curation, Writing - Original Draft, Visualization, Project administration, Funding acquisition. Pablo A. Prieto-Díaz: Methodology, Formal analysis, Software, Investigation, Writing - Original Draft. Marcos Vera: Conceptualization, Resources, Writing - Review & Editing, Supervision, Project administration, Funding acquisition.

Funding

This work has been partially funded by FEDER/MICINN-Agencia Estatal de Investigación under project TED2021-129378B-C21/AEI/10.13039/501100011033. A.A. Maurice acknowledges the support of an MCSF-Cofund “Energy for Future” postdoctoral research fellowship (E4F) from the Spanish Iberdrola Foundation (GA-101034297).

References

- [1] Z. Yang, J. Zhang, M. C. Kintner-Meyer, X. Lu, D. Choi, J. P. Lemmon, J. Liu, Electrochemical energy storage for green grid, *Chemical Reviews* 111 (5) (2011) 3577–3613. doi:10.1021/cr100290v.
- [2] B. Dunn, H. Kamath, J.-M. Tarascon, Electrical energy storage for the grid: a battery of choices, *Science* 334 (6058) (2011) 928–935. doi:10.1126/science.121274.
- [3] G. L. Soloveichik, Flow batteries: current status and trends, *Chemical Reviews* 115 (20) (2015) 11533–11558. doi:10.1021/cr500720t.
- [4] P. K. Leung, X. Li, C. Ponce de León, L. E. Berlouis, C. T. Low, F. C. Walsh, Recent developments in organic redox flow batteries: a critical review, *Journal of Power Sources* 360 (2017) 243–283. doi:10.1016/j.jpowsour.2017.05.057.
- [5] P. Alotto, M. Guarnieri, F. Moro, Redox flow batteries for the storage of renewable energy: A review, *Renewable and Sustainable Energy Reviews* 29 (2014) 325–335. doi:10.1016/j.rser.2013.08.001.
- [6] E. Sánchez-Díez, E. Ventosa, M. Guarnieri, A. Trovò, C. Flox, R. Marcilla, R. Ferret, Redox flow batteries: Status and perspective towards sustainable stationary energy storage, *Journal of Power Sources* 481 (2021) 228804. doi:10.1016/j.jpowsour.2020.228804.
- [7] X. G. Yang, Q. Ye, P. Cheng, T. S. Zhao, Effects of the electric field on ion crossover in vanadium redox flow batteries, *Applied Energy* 145 (2015) 306–319. doi:10.1016/j.apenergy.2015.02.038.
- [8] L. Wei, T. S. Zhao, Q. Xu, X. L. Zhou, Z. H. Zhang, In-situ investigation of hydrogen evolution behavior in vanadium redox flow batteries, *Applied Energy* 190 (2017) 1112–1118. doi:10.1016/j.apenergy.2017.01.039.
- [9] P. A. Prieto-Díaz, S. E. Ibáñez, M. Vera, Fluid dynamics of mixing in the tanks of small vanadium redox flow batteries: Insights from order-of-magnitude estimates and transient two-dimensional simulations, *International Journal of Heat and Mass Transfer* 216 (2023) 124567. doi:10.1016/j.ijheatmasstransfer.2023.124567.
- [10] K. Beyer, J. Grosse Austing, B. Satola, T. Di Nardo, M. Zobel, C. Agert, Electrolyte imbalance determination of a vanadium redox flow battery by potential-step analysis of the initial charging, *ChemSusChem* 13 (8) (2020) 2066–2071. doi:10.1002/cssc.201903485.

- [11] M. Skyllas-Kazacos, M. Kazacos, State of charge monitoring methods for vanadium redox flow battery control, *Journal of Power Sources* 196 (20) (2011) 8822–8827. doi:10.1016/j.jpowsour.2011.06.080.
- [12] P. Blanc, C. Madic, J. P. Launay, Spectrophotometric identification of a mixed-valence cation-cation complex between aquadioxovanadium(V) and aquaoxovanadium(IV) ions in perchloric, sulfuric, and hydrochloric acid media, *Inorganic Chemistry* 21 (8) (1982) 2923–2928. doi:10.1021/ic00138a003.
- [13] D. N. Buckley, X. Gao, R. P. Lynch, N. Quill, M. J. Leahy, Towards optical monitoring of vanadium redox flow batteries (vrfbs): An investigation of the underlying spectroscopy, *Journal of The Electrochemical Society* 161 (4) (2014) A524–A534. doi:10.1149/2.023404jes.
- [14] C. Petchsingh, N. Quill, J. T. Joyce, D. N. Eidhin, D. Oboroceanu, C. Lenihan, X. Gao, R. P. Lynch, D. N. Buckley, Spectroscopic measurement of state of charge in vanadium flow batteries with an analytical model of V^{IV} - V^V absorbance, *Journal of The Electrochemical Society* 163 (1) (2016) A5068–A5083. doi:10.1149/2.0091601jes.
- [15] L. Liu, J. Xi, Z. Wu, W. Zhang, H. Zhou, W. Li, X. Qiu, State of charge monitoring for vanadium redox flow batteries by the transmission spectra of V(IV)/V(V) electrolytes, *Journal of Applied Electrochemistry* 42 (12) (2012) 1025–1031. doi:10.1007/s10800-012-0477-2.
- [16] Z. Tang, D. S. Aaron, A. B. Papandrew, T. A. Zawodzinski, Monitoring the state of charge of operating vanadium redox flow batteries, *ECS Transactions* 41 (23) (2012) 1–9. doi:10.1149/1.3697449.
- [17] W. Zhang, L. Liu, L. Liu, An on-line spectroscopic monitoring system for the electrolytes in vanadium redox flow batteries, *RSC Advances* 5 (121) (2015) 100235–100243. doi:10.1039/C5RA21844F.
URL <http://xlink.rsc.org/?DOI=C5RA21844F>
- [18] K.-H. Shin, C.-S. Jin, J.-Y. So, S.-K. Park, D.-H. Kim, S.-H. Yeon, Real-time monitoring of the state of charge (SOC) in vanadium redox-flow batteries using UV–Vis spectroscopy in operando mode, *Journal of Energy Storage* 27 (2020) 101066. doi:10.1016/j.est.2019.101066.
- [19] P. Loktionov, R. Pichugov, D. Konev, M. Petrov, A. Pustovalova, A. Antipov, Operando UV/Vis spectra deconvolution for comprehensive electrolytes analysis of vanadium redox flow battery, *Journal of Electroanalytical Chemistry* 925 (2022) 116912. doi:10.1016/j.jelechem.2022.116912.
- [20] A. A. Maurice, A. E. Quintero, M. Vera, A comprehensive guide for measuring total vanadium concentration and state of charge of vanadium electrolytes using UV-Visible spectroscopy, *Electrochimica Acta* (2024) 144003. doi:10.1016/j.electacta.2024.144003.
- [21] L. Liu, Z. Li, J. Xi, H. Zhou, Z. Wu, X. Qiu, Rapid detection of the positive side reactions in vanadium flow batteries, *Applied Energy* 185 (2017) 452–462. doi:<https://doi.org/10.1016/j.apenergy.2016.10.141>.
URL <https://www.sciencedirect.com/science/article/pii/S0306261916314805>

- [22] K. Schofield, P. Musilek, State of charge and capacity tracking in vanadium redox flow battery systems, *Clean Technologies* 4 (3) (2022) 607–618. doi:10.3390/cleantechnol4030037. URL <https://www.mdpi.com/2571-8797/4/3/37>
- [23] D. Li, Y. Zhang, Z. Li, L. Liu, A low-cost average valence detector for mixed electrolytes in vanadium flow batteries, *RSC Adv.* 8 (37) (2018) 20773–20780, publisher: The Royal Society of Chemistry. doi:10.1039/C8RA02598C. URL <http://dx.doi.org/10.1039/C8RA02598C>
- [24] S. Rudolph, U. Schröder, I. Bayanov, K. Blenke, D. Hage, High resolution state of charge monitoring of vanadium electrolytes with IR optical sensor, *Journal of Electroanalytical Chemistry* 694 (2013) 17–22. doi:10.1016/j.jelechem.2013.01.042. URL <https://linkinghub.elsevier.com/retrieve/pii/S1572665713000763>
- [25] Raspberry Pi Foundation, Raspberry Pi, <https://www.raspberrypi.com> (2025).
- [26] P. A. Prieto-Díaz, A. A. Maurice, M. Vera, Measuring density and viscosity of vanadium electrolytes: A database with multivariate polynomial fits, *Journal of Energy Storage* 94 (2024) 112429. doi:<https://doi.org/10.1016/j.est.2024.112429>. URL <https://www.sciencedirect.com/science/article/pii/S2352152X24020152>
- [27] AMS-OSRAM, As7341 datasheet: 11-channel spectral sensor with flicker detection and nir channel, <https://look.ams-osram.com/m/24266a3e584de4db/original/AS7341-DS000504.pdf>, accessed: 4 January 2025 (January 2025).
- [28] K. Deep, K. P. Singh, M. Kansal, C. Mohan, A real coded genetic algorithm for solving integer and mixed integer optimization problems, *Applied Mathematics and Computation* 212 (2) (2009) 505–518. doi:doi.org/10.1016/j.amc.2009.02.044.